Advance Sustainable Science, Engineering and Technology (ASSET)
Vol. 8, No.2, April 2026, pp. 02602027-01 ~ 02602027-018
ISSN: 2715-4211 DOI: https://doi.org/10.26877/asset.v8i2.2740

Microwave-Pyrolysed Rice Husk-Derived Activated Carbon as a Sustainable Anode Material for Lithium-Ion Half-Cell Batteries

Nur Atiqah Surib[1,2], Muhammad Amirul Aizat Mohd Abdah[3,4*], Farhana Syakirah Ismail[2], Wong Weng Pin[2], Farah Ezzah Ab Latif[2], Muhammad Norhaffis Mustafa[2], Rashmi Walvekar[5,6], Mohammad Khalid[7,8,9*]

[1]Department of Materials and Life Sciences, Sophia University, 7-1 Kioi-cho,
Chiyoda-ku, Tokyo, 102-8554 Japan.

[2]Sunway Centre for Electrochemical Energy and Sustainable Technology (SCEEST),
School of Engineering and Technology, Sunway University, No. 5 Jalan Universiti,
Bandar Sunway, 47500 Petaling Jaya, Selangor, Malaysia

[3]Department of Chemistry, Faculty of Sciences, University Teknologi Malaysia,
81310 UTM Johor Bahru, Johor, Malaysia

[4]Advanced Membrane Technology Research Centre, Faculty of Chemical and Energy
Engineering, Universiti Teknologi Malaysia, 81310 Skudai, Johor, Malaysia

[5]FDepartment of Chemical and Process Engineering, University of Strathclyde G1
1XL, UK

[6]Research and Innovation Cell, Bahra University, Distt. Solan, HP, Waknaghat, India

[7]Materials and Manufacturing Research Group, James Watt School of Engineering,
University of Glasgow, Glasgow G12 8QQ, UK

[8]Faculty of Engineering, Manipal University Jaipur, Rajasthan, 303007, India

[9]University Centre for Research and Development, Chandigarh University, Mohali,
Punjab, 140413, India

*muhammadamirulaizat@utm.my

Abstract. Agricultural waste biomass is explored as a sustainable precursor for activated carbon. In this study, rice husk-derived activated carbon (RHAC) was synthesized via microwave-assisted pyrolysis and KOH activation at 600, 700, and 800 °C. The KOH activation enhanced the thermal stability of the samples, with RHAC_700 exhibiting a spongy, interconnected structure and a surface area of 390.33 $m^2 g^{-1}$. When evaluated as a half-cell anode materials for lithium-ion batteries, RHAC_700 delivered an initial discharge capacity of approximately 388.33 ± 11.65 mAh g^{-1} with Coulombic efficiency 68.29 % and stabilized at 250.00 ± 7.33 mAh g^{-1} with 99.82% of Coulombic efficiency after 100 cycles at 0.2 A g^{-1} and 25 °C (active material loading: 0.95 ± 0.15 mg cm^{-2}). All reported values represent the average of three independent cells. Furthermore, RHAC_700 demonstrated good rate capability, retaining capacities from 248.33 ± 7.45 mAh g^{-1} to 134.58 ± 4.04 mAh g^{-1} at current densities ranging from 0.2 to 1.0 A g^{-1}.

Keywords: biomass-derived carbon, microwave pyrolysis, sustainable anode, koh activation, lithium-ion batteries.

(Received 2025-09-15, Revised 2025-12-31, Accepted 2026-01-13, Available Online by 2026-04-26)

1. Introduction

Over the past decades, carbon materials, particularly graphite, have been widely used as anode materials in lithium-ion batteries owing to their stable structure, good electrical conductivity, and long cycle life [1, 2]. However, graphite suffers from intrinsic limitations, including a relatively low theoretical capacity of 372 mAh g^{-1} and limited rate capability, restricting its suitability for applications requiring both high power and high energy density [3]. Therefore, the exploration of new carbonaceous materials and their effective utilization as anodes in lithium-ion batteries offers a significant opportunity for advancing the next-generation lithium-ion battery technology.

Significant research efforts have been dedicated to explore and developing activated carbon anodes derived from various agricultural wastes. This is owing to features such as rich surface functional groups and a wide range of pore size distributions, which enable more active sites for charge accumulation and enhance capacity [4, 5]. Among various biomass precursors, rice husk has attracted considerable attention due to its high availability, renewability, and cost-effectiveness. Rice husk is a byproduct generated during the dehusking process at rice mills and consists mainly of cellulose (33%), hemicellulose (26%), lignin (22%), SiO_2, and a small amount of ash. Its relatively high carbon content (37–54%) makes rice husk an attractive and sustainable precursor for the synthesis of carbon-based electrode materials [6-8].

Recent studies have demonstrated the potential of rice husk-derived carbon materials for lithium-ion battery applications, predominantly prepared via conventional furnace-based pyrolysis and chemical activation routes [9]. For instance, Angellinov et al. (2025) employed rice husk-derived activated carbon as a coating layer on NMC 811 cathodes to enhance electronic conductivity and structural stability. In their work, rice husk carbon was first obtained by carbonization in a closed chamber at 400 °C for 4 h, followed by chemical activation with NaOH and subsequent heat treatment under nitrogen at 850 °C for 2 h. The addition of 5 wt% rice husk-derived activated carbon to the NMC 811 electrode resulted in a substantial increase in electrical conductivity, from 1.5951×10^{-5} S cm^{-1} to 1.4324×10^{-4} S cm^{-1}, alongside an improvement in specific capacity from 16.30 mAh g^{-1} to 44.51 mAh g^{-1} [10]. Similarly, Nilmoung et al. (2024) evaluated the electrochemical performance of rice husk-activated carbon (RHAC) composited with V_2O_5 as a cathode material for lithium-ion batteries. The RHAC/V_2O_5 composite, prepared by carbonization at 800 °C for 3 h under an argon atmosphere with 10% NaOH impregnation, delivered a specific capacity of 186 mAh g^{-1} at 0.2 C after 100 cycles [11]. Moreover, Hou et al. (2021) showed that rice husk-derived hard carbon obtained via 24 h hydrothermal treatment displayed a large surface area and delivered a specific capacity of 679.9 mAh g^{-1} after 100 cycles at 0.2 C [12]. Collectively, these studies confirm the electrochemical potential of rice husk-derived carbons in lithium-ion battery systems.

Despite these encouraging outcomes, the synthesis strategies employed in most reported studies share common limitations. Conventional pyrolysis and chemical activation processes are inherently energyintensive, requiring high processing temperatures and prolonged treatment durations. Moreover, heat transfer in these processes is externally driven, often resulting in non-uniform temperature distributions and limited control over pore homogeneity [13, 14]. These drawbacks present significant challenges for the scalable, energy-efficient, and sustainable production of biomass-derived carbon anodes.

To overcome these limitations, microwave-assisted pyrolysis has emerged as an attractive alternative for converting biomass into activated carbon, offering rapid volumetric heating, shortened processing times, and potentially reduced energy consumption compared with traditional furnace-based methods [14, 15]. The characteristics of carbon materials produced via microwave-assisted pyrolysis are strongly governed by several key processing parameters, including microwave power, irradiation time, heating rate, and the dielectric properties of the precursor material [16, 17]. Microwave power and exposure duration directly influence the extent of carbonization, volatile release, and defect formation, thereby affecting pore development and structural ordering [18]. In addition, the intrinsic dielectric response of biomass components determines the efficiency of microwave energy absorption and internal heat generation, which can lead to variations in temperature distribution and carbon microstructure. Careful control of these parameters is therefore essential to achieve reproducible carbon yields, tailored pore architectures, and stable electrochemical performance in microwave-derived carbons [19, 20].

Despite increasing interest in microwave-assisted pyrolysis as an energy-efficient approach for converting biomass into carbon materials, its combined use with subsequent chemical activation for lithium-ion battery anode applications remains limited, particularly for rice husk-derived carbons. Most reported studies rely exclusively on either conventional furnace-based carbonization and activation or microwave treatment alone, while systematic investigations integrating microwave-assisted pyrolysis for carbon precursor preparation followed by KOH activation at controlled temperatures in a tube furnace are still scarce. Furthermore, the influence of activation temperature on pore structure evolution, electrochemical reversibility, and long-term cycling stability of rice husk-derived carbon anodes prepared via this hybrid route has not been comprehensively addressed.

In this work, we propose a hybrid synthesis strategy in which rice husk is first converted into carbon via microwave-assisted pyrolysis and subsequently activated using KOH in a tube furnace at different temperatures. The primary objective is to develop a structurally stable carbon anode with good cycling stability and high coulombic efficiency. Among the investigated samples, the RHAC prepared at 700 °C exhibits the most balanced electrochemical performance, delivering an initial discharge capacity of approximately 388.33 ± 11.65 mAh g^{-1} and stabilizing at 250.00 ± 7.33 mAh g^{-1} after 100 cycles with a Coulombic efficiency of 99.82%, outperforming the materials activated at 600 °C and 800 °C. These results indicate that the combined use of microwave-assisted pyrolysis and temperature-controlled KOH activation provides a promising route for producing rice husk-derived activated carbon with potential as an anode material for lithium-ion batteries.

2. **Methods**

2.1. Materials

Rice husk (RH) was purchased from a local supplier. Lithium fluoride (LiF, ~300 mesh) powder and 1.0 M lithium hexafluorophosphate (designated as $LiPF_6$) in ethylene carbonate and dimethyl carbonate (EC: DMC; 1:1 by volume) were obtained from Sigma-Aldrich. *N*,*N*-Dimethylformamide (DMF), and Solef®polyvinylidene fluoride (PVDF) were acquired from R&M Chemicals and Solvay Specialty Chemicals Asia Pacific Pte Ltd., Singapore, respectively. Ethanol (EtOH, 96 %) and hydrochloric acid (HCl, 37 % *v*/*v*) were acquired from Fisher Scientific. Super P® carbon and copper (Cu) foil were purchased from KGC Resources Sdn. Bhd., Malaysia. Celgard® polypropylene membranes were obtained from Xiamen AOT Electronic Technology Co., Ltd. Deionized (DI) water (18.2 MΩ.cm) from the Adrona Crystal EX was utilized in all experiments. All reagents utilized in this study were of analytical grade and used as received without further purification.

2.2. *Synthesis of rice husk activated carbon (RHAC)*

The synthesis of rice husk activated carbon consists of three steps: preliminary treatment, pyrolysis and chemical activation. In preliminary treatment, rice husk (RH) used as the carbon precursor, was first rinsed with tap water and subjected to 20 min of sonication to remove dust and other contaminants. It was then washed with deionized (DI) water to eliminate any residual tap water impurities and dried at 110 °C for 12 h. The dried RH was ground into a fine powder using a commercial blender. Approximately 0.5 g of the RH powder was mixed with 5 mL of 3.5 M HCl in a cylindrical Teflon tube reactor. Subsequently, microwave-assisted pyrolysis of the rice husk was carried out without Ar flow in a flexiWAVE microwave-assisted hydrothermal reactor (flexiWAVE Milestone, Italy) at 230 °C, with a power of 800 W, a heating rate of 11.5 °C min^{-1} and a holding time of 25 min. This process transformed the rice husk into carbon, designated as RHC. Subsequently, the produced RHC was then centrifuge at 10,000 rpm for 5 min followed by drying at 100 °C for 24 h. The dried RHC was ground into a fine powder using a mortar and pestle. For chemical activation, RHC powder was mixed with aqueous KOH solution at a 1:3 weight ratio (KOH:RHC), magnetically stirred at 300 rpm for 3 h at room temperature. The mixture was dried overnight at 100 °C in a vacuum oven, followed by activation in a tube furnace under Ar flow (100 mL min^{-1}) at different temperatures (600 °C, 700 °C, 800 °C) with a holding time of 2 h and heating rate 5 °C min^{-1}. After cooling, the rice husk activated carbon sample (RHAC) was neutralized with 0.5 M HCl until reaching a pH value of approximately 6-7 and then washed with distilled water. Subsequently, the RHAC sample was centrifuged at 10 000 rpm for 5 min followed by drying in oven at 80 °C overnight. The obtained RHAC samples were denoted as RHAC_600, RHAC_700, and RHAC_800, corresponding to the activation temperatures of 600 °C, 700 °C, and 800 °C, respectively. Each synthesis condition was repeated in three independent runs to ensure reproducibility. The mass yields were calculated based on Equation 1 and reported in Table S1.

$$Yield\,(\%) = \frac{M_f}{M_i} \times 100 \tag{1}$$

where M_f is the final weight and M_i is the initial weight of the sample. The mass yields obtained for RHC, RHAC_600, RHAC_700 and RHAC_800 were 93 %, 25 %, 24 % and 23 % respectively.

2.3. *Physicochemical characteristics*

The morphology and microstructure were investigated through a FEI Quanta FEG 400 field emission scanning electron microscope (FESEM) equipped with an energy-dispersive X-ray spectrometer (EDX). The crystal phases and carbon nature of the synthesized samples were characterized using X-ray diffraction (XRD) analysis (Bruker D8 Advance using Cu Kα as the X-ray source (λ = 1.54 Å). The specific surface area and pore size distribution were determined by N_2 adsorption and desorption using Micromeritics Smart VacPrep and Micromeritics 3Flex physisorption analyzer equipped with a cryostat at 77 K. Barret–Joyner–Halinda (BJH) method was employed to calculate pore volume and pore size distribution. Raman spectroscopy was performed using a DXR 2xi Raman imaging microscope using a 532 nm Ar-ion laser. Raman spectra were recorded using WITec Raman spectroscope with a green laser (excitation wavelength: 532 nm). Thermogravimetric analysis (TGA) was conducted on rice husks both before and after activation, utilizing a TGA instrument (TGA 209 F3 Tarsus, NETZSCH) under a nitrogen (N_2) atmosphere with a heating rate of 10 °C min^{-1}.

2.4. *Electrochemical characterizations*

In the fabrication of RHAC electrodes, the working electrode was prepared by grinding and mixing active materials (RHAC powder), carbon additive (Super P®) and polymeric binder (PVDF) in DMF solvent at a weight ratio of 85:5:10 to obtain a uniform slurry. Next, the mixed slurry was coated onto a Cu foil using a doctor blade with a thickness of 150 mm. All electrodes were fabricated following the same slurry composition, coating procedure, and drying conditions to ensure good reproducibility and comparable active material mass loadings. After drying under vacuum at 100 °C, the electrodes were used directly without further calendering or pressing. The average mass loading of the active material was 0.95 ± 0.15 mg cm^{-2} (range: 0.72–1.17 mg cm^{-2}, n = 9). The electrodes were punched into 16 mm diameter discs (area: 2.01 cm^2) and dried overnight in a vacuum oven at 80 °C prior to half-cell assembly.

Electrochemical testing was conducted using CR2023 coin cells assembled in an Ar-filled glovebox (O_2 < 0.1 ppm). Each half-cell used Li metal (15.6 mm × 0.25 mm) as counter /reference electrode, a Celgard 2400 membrane served as the separator and the electrolyte used was composed of 1.0 M $LiPF_6$ in EC/DMC (1:1 by volume). An electrolyte volume of 80 µL was used for each cell, and the separator was soaked with the electrolyte for 15 s prior to cell assembly. Coin cells were crimped at 0.4 MPa to ensure a secure seal. For each sample, three independent coin cells were assembled and tested (n = 3). The reported electrochemical data represent the average values obtained from these independent measurements, with cell-to-cell variation in specific capacity within ±5 %. Figure 1 illustrates the overview of synthesizing rice husk activated carbon as anode material in lithium-ion battery. Cyclic voltammetry (CV) measurements were conducted in the voltage range of 0.1 to 3.0 V (*vs.* Li/Li^+) at a scan rate of 0.1 mV s^{-1}. Electrochemical impedance spectroscopy (EIS) was performed with an AC oscillation of 5 mV over a frequency range from 1 MHz to 0.1 Hz. The CV and EIS analyses were conducted using a potentiostat/galvanostat (Princeton Applied Research, Model. VersaSTAT 4) electrochemical station. The galvanostatic discharge/charge (GCD) tests were conducted using a NEWARE-BTS4000-5V10mA Battery Testing System within the voltage range of 0.01–2.0 V (*vs.* Li/Li^+) at 0.2 A g^{-1}. The specific capacity and current density of the completed coin cell were determined by considering the mass of the active material present in the electrode. All the electrochemical measurements were performed at room temperature (25 °C).

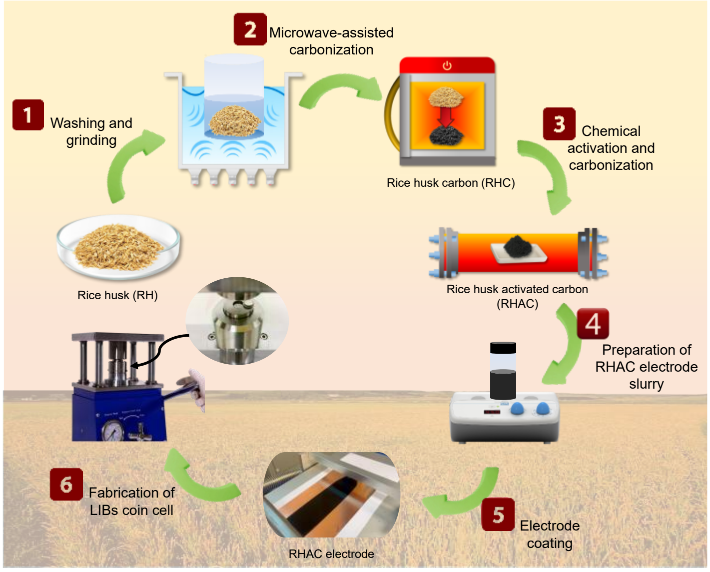

Figure 1. Schematic illustration of rice husk–derived activated carbon coin cell fabrication

3. Results and Discussion

3.1. Surface morphology characterization

Figure 2 displays the FESEM morphology of RH, RHC and RHAC samples activated at 600 °C, 700 °C, and 800 °C (RHAC_600, RHAC_700 and RHAC_800). Figure 2 (a) shows that the RH sample was composed of agglomerated spherical particles with diameter of around 0.293 to 0.329 µm. After the raw rice husk underwent microwave-assisted pyrolysis, a rough morphology with few porous structures around 0.3 µm sizes was observed on the surface of RHC sample, as shown in Figure 2 (b). During the microwave-assisted pyrolysis process, the cellulose and hemicellulose present in the rice husk underwent incomplete decomposition into small volatile molecules, which then escaped from the surface. This phenomenon led to the formation of a porous structure on the RHC sample [21].

Figure 2 (c-e) show progressive pore development on RHAC surfaces with increasing activation temperature from 600 °C to 800 °C. This finding demonstrates that as the activation temperature increases, the organic components in the RH will undergo complete pyrolysis, resulting in the creation of additional pores on the RHAC samples [22]. During the activation process, the reaction between KOH and carbon is believed to generate gases that promote the creation of pores [23]. Among the three RHAC samples, RHAC_600 sample had the fewest and largest pore size, around 0.9-1.0 µm. The surface of the RHAC_700 sample exhibited a spongy structure with uniform size ranging from 0.2 to 0.3 µm. Upon reaching a higher activation temperature, the surface of RHAC_800 showed an irregular porous structure ranging from 0.1 to 0.3 µm in size. This may be attributed to the collapse of the pores that occurred due to the high temperature, which could affect the performance. The presence of a spongy structure in RHAC_700 sample shows the potential for the material to be used as anode material in lithium-ion battery. The porous structure serves as a pathway for lithium ions (0.069 nm) and electrons, minimizing the volume expansion of the material during the insertion of lithium ions, ultimately improving cycle performance [12]. This is in accordance with the charge-discharge results shown in Figure 6. The elemental analysis of the RHAC_700 sample is presented in Figure 2 (f). Based on the EDX measurement, the relative composition of RHAC_700 sample was 84.55 % carbon, 15.05 % oxygen, 0.08 % silica, 0.14 % chlorine, and 0.17 % potassium.

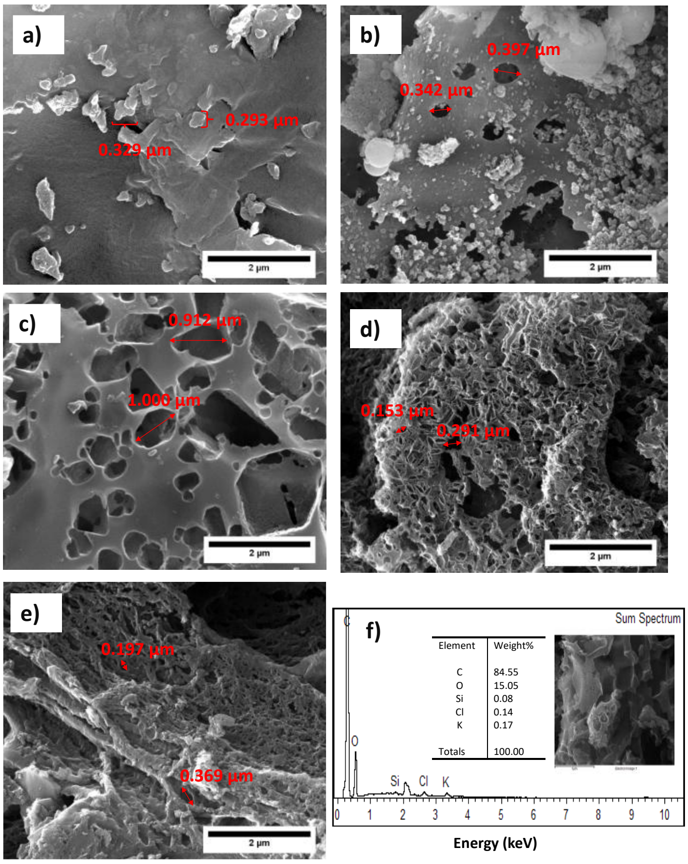

Figure 2. FESEM morphology images of samples (a) RH, (b) RHC, (c) RHAC_600, (d) RHAC_700, (e) RHAC_800 under magnification 50 000X and (f) the EDX spectrum of RHAC_700 sample

3.2. *Brunauer Emmett Teller analysis*

Figure 3 (a-c) show the N_2 adsorption–desorption isotherms of the carbonaceous materials, while the corresponding textural parameters, including the BET surface area, total pore volume, and average pore size, are summarized in Table 1. The N_2 adsorption–desorption isotherm of raw rice husk (RH) is nearly flat over the entire relative pressure range, indicating a very low N_2 uptake. This is consistent with its extremely small BET surface area (0.7728 $m^2\ g^{-1}$) and pore volume (0.0054 $cm^3\ g^{-1}$), confirming a largely nonporous or poorly accessible structure. After microwave-assisted pyrolysis, rice husk carbon (RHC) shows a modest increase in the adsorbed volume and BET surface area (33.1687 $m^2\ g^{-1}$), suggesting the initial formation of micro- and mesopores due to the removal of volatile components during carbonization [23]. A pronounced structural transformation occurs after KOH activation at 700 °C (RHAC_700). The adsorption isotherm evolves into a typical Type IV profile with a clear hysteresis loop, reflecting abundant micro- and mesoporosity [24]. Accordingly, the BET surface area and pore volume increase substantially to 390.3280 $m^2\ g^{-1}$ and 0.1521 $cm^3\ g^{-1}$, respectively, indicating the formation of an interconnected porous network.

The pore diameter distributions in Figure 3 (c) further support this trend. RH exhibits an extremely low pore volume across all pore sizes, while RHC shows increased pore volume mainly in the mesopore range (10–50 nm). In contrast, RHAC_700 displays a dominant mesoporous distribution with significantly higher pore volume, confirming that KOH activation effectively tailors the pore structure [25]. This optimized mesoporous is expected to facilitate electrolyte penetration and ion transport, thereby contributing to the improved electrochemical performance of RHAC_700 as a lithium-ion battery anode.

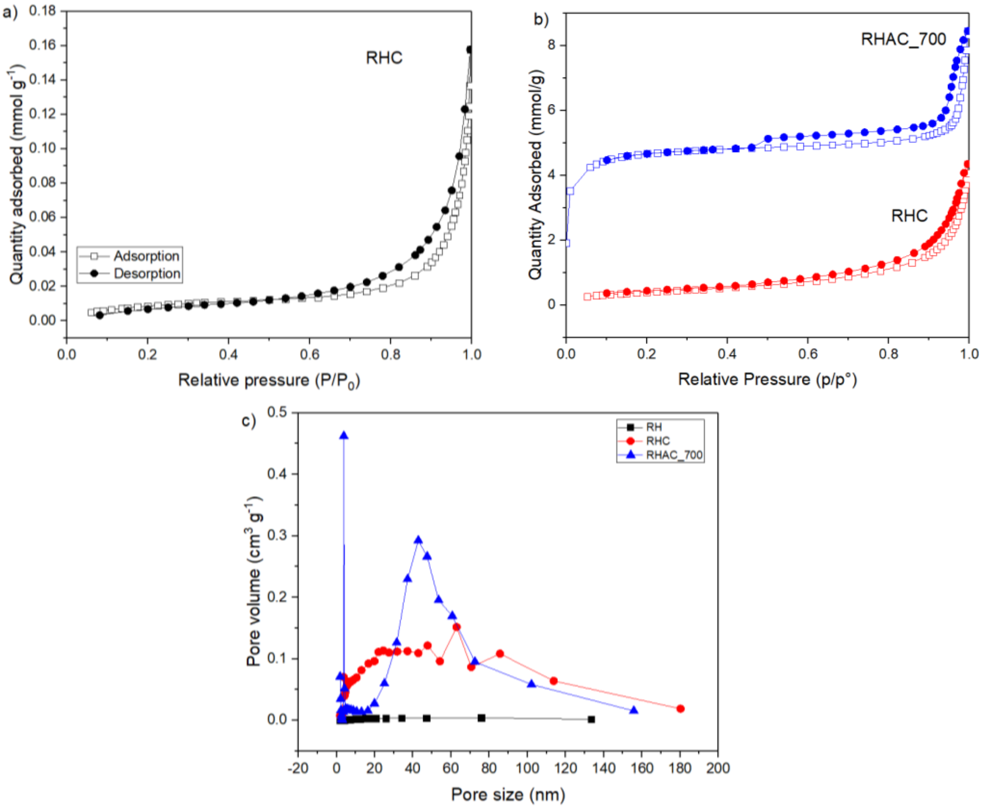

Figure 3. (a-b) Adsorption and desorption isotherm of RH, RHC and RHAC_700 samples and (c) BJH pore size distribution.

Table 1. Surface area, BJH pore volume and BJH pore size of RH, RHC and RHAC samples

Sample	**BET surface area (m^2/g)**	**Pore volume (cm^3/g)**	**Pore size (nm)**
RH	0.7728	0.0054	24.9932
RHC	33.1687	0.1515	15.8261
RHAC-700	390.3280	0.1521	12.0715

3.3. X-ray diffraction and Raman analysis

The X-ray diffraction patterns of RH, RHC and RHAC samples prepared at different activation temperatures are presented in Figure 4 (a). The RH sample exhibits diffraction peaks at 16 °, 22 ° and 35 °, which are attributed to the peaks of cellulose with crystallographic planes (10-1), (002) and (040), respectively (JCPDS 03-0289) [26, 27]. Additionally, a broad peak in the range of 18–30 ° is attributed to silica with an amorphous nature [26]. In the RHC sample, a broad peak observed between 17-30 ° is assigned to amorphous carbon [26]. For RHAC sample activated at different temperatures, the presence of two peaks at 23 ° and 43 ° corresponds to the (002) and (100) reflections of the disordered carbon layer, respectively [28, 29]. The broad peak observed at approximately 23 ° is due to the existence of amorphous and turbostratic carbon [22]. The weak and broad peak located at approximately 43 ° corresponds to the honeycomb structure generated by the arrangement of sp^2 hybridized carbon atoms [30]. As the activation temperature increases, the (002) plane reflections around 30 ° become relatively narrow and stronger, implying that high temperatures can enhance the degree of graphitization of the carbon material [31].

Raman spectroscopy analysis was carried out in order to gain deeper understanding of the internal structure, including the degree of crystallinity and disordering of the activated carbon derived from rice husk. Figure 4 (b) shows that all the samples exhibit two prominent peaks near 1350 cm^{-1} and 1580 cm^{-1}, corresponding to the D and G bands, respectively [30]. The presence of the D band indicates the existence of structural defects in the carbon materials, while the G band is associated with the vibration of sp^2-hybridized carbon atoms in graphite sheets [32]. Generally, the ratio between the intensities of the D and G band (I_d/I_g) signifies the degree of material defects. The lower intensity ratio indicates a higher degree of crystallinity and fewer defects in the carbon structure [33]. The calculated I_d/I_g ratios for RHC, RHAC_600, RHAC_700, and RHAC_800 are 1.02, 0.60, 0.85 and 0.57, respectively. These results indicate that the RHAC samples generally exhibit a more ordered and graphitic structure with increasing activation temperature, which is consistent with the XRD results. However, the I_d/I_g ratio of RHAC_700 sample is 0.85, which is higher than that of the RHAC_600 and RHAC_800 samples, indicating that the sample has more defects in the carbon structure. These defects may provide additional electrochemical active sites, thereby enhancing the reaction kinetics on the material surface and consequently increasing lithium-ion storage capacity [30, 34].

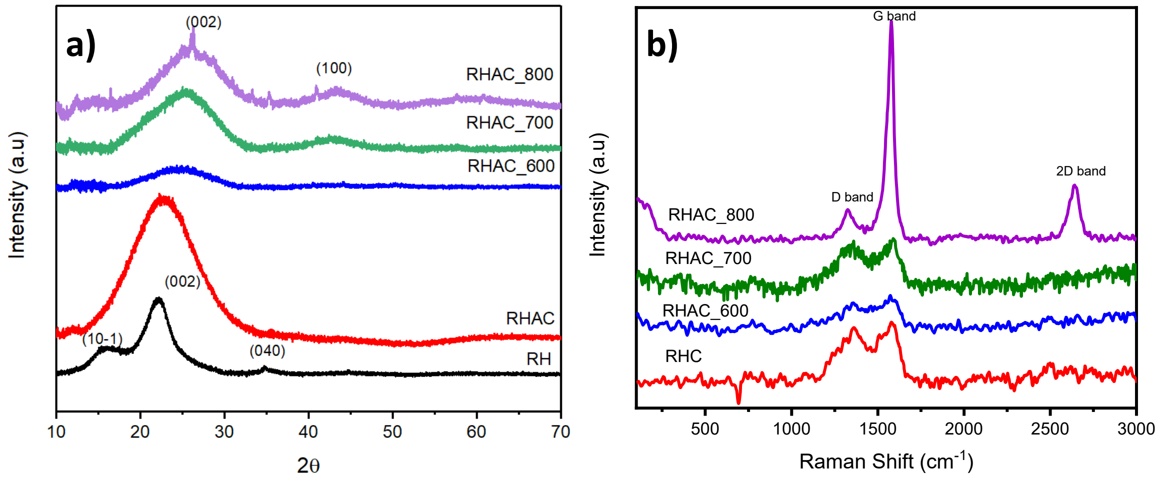

Figure 4. (a) XRD patterns for RH, RHC, RHAC_600, RHAC_700, and RHAC_800 samples (b) Raman spectrum of RHC and RHAC_600, RHAC_700, and RHAC_800 samples

3.4. Thermal Analysis

Figure 5 displays the thermogravimetric analysis results for the RH, RHC, RHAC_600, RHAC_700, and RHAC_800 samples. The weight loss curve can be divided into three distinct stages. The initial decrease in sample weight between 40 and 150 °C is attributed to the presence of moisture in the sample. The main region of mass loss is observed within the temperature range between 200 – 380 °C, corresponding to the decomposition of hemicellulose, cellulose and waxy substances [35]. At temperatures above 380 °C, further weight loss is attributed to the degradation of lignin [36]. The RH sample exhibits the largest weight loss, primarily due to the release of volatile substances such as H_2O, H_2, and CO [22]. The weight loss gradually decreased as the RH sample underwent microwave-assisted pyrolysis followed by activation at increasing temperatures. This trend is attributed to the progressive reduction of volatile components and the enhancement of thermal stability with increasing activation temperature [37].

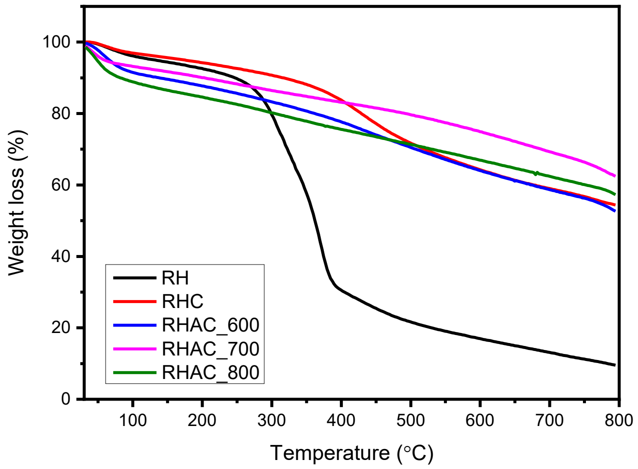

Figure 5. TGA curve for RH, RHC, RHAC_600, RHAC_700, and RHAC_800 samples

3.5. *Electrochemical properties in lithium-ion batteries*

The electrochemical performance of RHAC electrodes was investigated using lithium-ion half-cell configurations, with RHAC as an anode and Li metal as the counter electrode. Figure 6 (a) shows the CV curve of RHAC_700 electrodes conducted in the voltage range of 0.1 to 3.0 V (*vs.* Li/Li^+) at a scan rate of 0.1 mV s^{-1}. In the first cycle, a reduction peak appears in the potential range of 0-0.2V, which is ascribed to the lithium-ion intercalation into the carbon layers or lithium storage within the pores. The reduction peak at 1.5 V is attributed to the reaction of lithium ions with oxygen-containing functional groups on the electrode surface [38]. The peak observed in the range of 0.3–1.2 V is associated with electrolyte decomposition and the formation of the solid electrolyte interphase (SEI) film on the anode surface [30, 39]. The presence of an oxidation peak at 0.2–0.5 V corresponds to the deintercalation of lithium ions [12]. In addition, the CV curve overlaps well after the second cycle, indicating that the RHAC_700 electrode exhibits good electrochemical reversibility [40].

The galvanostatic charge–discharge (GCD) performance of the lithium half-cells was evaluated in the voltage range of 0.01–2.0 V at a current density of 0.2 A g^{-1}. Figure 6 (b) shows the cycling performance of the RHAC_600, RHAC_700, and RHAC_800 electrodes, while Figure 6 (c) presents the corresponding coulombic efficiency. The discharge specific capacity and Coulombic efficiency are reported as mean values from three independently assembled cells (n = 3), with error bars representing the standard deviation (±SD).

All samples exhibit relatively high initial discharge capacities during the first few cycles, followed by a rapid capacity decay, which is a characteristic behavior of biomass-derived carbon anodes in lithium-ion batteries. As shown in Figure 6 (b), the RHAC_800 electrode delivers the highest initial discharge capacity of 410.00 ± 12.30 mAh g^{-1}, compared with RHAC_700 (388.33 ± 11.65 mAh g^{-1}) and RHAC_600 (217.91 ± 6.54 mAh g^{-1}). The corresponding first-cycle Coulombic efficiencies (CEs) for RHAC_600, RHAC_700, and RHAC_800 are 75.62 %, 76.29 %, and 68.29 %, respectively.

The pronounced initial irreversible capacity loss observed for all RHAC samples can be attributed to multiple factors. First, the presence of silicon species detected by EDX analysis may partially contribute to the high initial discharge capacity through lithium–silicon alloying reactions during the early cycles. Previous studies have shown that Si-based anodes are prone to SEI instability because the substantial volume expansion and contraction of silicon during repeated lithiation and delithiation continuously disrupt the SEI layer. This repeated SEI breakdown and reformation leads to increased SEI thickness and accelerated electrolyte consumption, ultimately hindering lithium-ion transport and degrading electrode integrity [41]. In addition, a significant amount of lithium ions is consumed during SEI formation and electrolyte decomposition involving carbonate-based solvents during the first discharge cycle [42-44]. Furthermore, owing to the amorphous nature of the carbon structure and the heterogeneous distribution of active sites, not all inserted lithium ions can be reversibly extracted during the initial cycles, resulting in a lower first-cycle Coulombic efficiency [33]. Additionally, oxygen-containing functional groups prevalent in biomass-derived carbons like RHAC can contribute to extra capacity via surface Li^+ adsorption and reversible redox at defect/edge sites, but they also promote excessive SEI formation and partial irreversibility during initial cycles. These polar groups interact strongly with Li^+, forming surface complexes that add pseudocapacitive sloping capacity, yet trap some ions irreversibly alongside electrolyte decomposition [45].

After the initial stabilization period (approximately 20–30 cycles), all electrodes exhibit stable cycling behavior with small SD values, indicating good cell-to-cell reproducibility. For instance, at the 50th cycle, RHAC_600, RHAC_700, and RHAC_800 deliver average discharge capacities of 134.03 ± 4.03 mAh g^{-1} (CE: 97.31%), 263.75 ± 7.91 mAh g^{-1} (CE: 97.31%), and 156.00 ± 4.68 mAh g^{-1} (CE: 98.29%), respectively.

Notably, the RHAC_700 electrode consistently exhibits the highest reversible capacity and good cycling stability, maintaining a discharge capacity of 250.00 ± 7.33 mAh g^{-1} with a Coulombic efficiency of 99.82 % after 100 cycles, compared with RHAC_600 (137.01 ± 4.11 mAh g^{-1}, CE: 98.91 %) and RHAC_800 (154.67 ± 4.64 mAh g^{-1}, CE: 99.57 %). The enhanced electrochemical performance of RHAC_700 can be attributed to its spongy and interconnected porous structure, as observed in the

FESEM image (Figure 2), which provides abundant active sites for lithium-ion storage and facilitates efficient electron and ion transport within the electrode, thereby improving the overall cycling performance [23]. In contrast, the slightly lower capacity of RHAC_800 is likely due to over-activation at the higher KOH treatment temperature, which causes partial pore collapse as observed in the FESEM images. Additionally, the lower I_d/I_g ratio indicates a more graphitized but less defective structure, meaning that fewer active sites are available for lithium-ion storage, thereby limiting the overall capacity despite reasonable conductivity [12, 22].

The performance of the RHAC_700 was examined at different current densities ranging from 0.2 to 1.0 A g^{-1} for 20 cycles, as depicted in Figure 6 (d). As the current density increased from 0.2 A g^{-1} to 1.0 A g^{-1}, the average discharge specific capacity decreased from 248.33 ± 7.45 mAh g^{-1} to 134.58 ± 4.04 mAh g^{-1} . At higher current densities, ion transport within the electrolyte is limited by diffusion constraints, which prevent lithium ions from reaching all available active sites on the RHAC_700 surface. As a result, the discharge specific capacity decreases with increased current density [46]. When the current density was returned to 0.2 A g^{-1}, the discharge specific capacity recovered to 245 ± 7.35 mAh g^{-1}, demonstrating good electrochemical reversibility of the material [40].

Table 2 compares the electrochemical performance of various carbonaceous anodes. Our RHAC_700 sample delivers a discharge specific capacity of 250.00 ± 7.33 mAh g^{-1} at 0.2 A g^{-1} after 100 cycles with a Coulombic efficiency of 99.82%, highlighting its potential as a sustainable anode material for lithium-ion batteries.

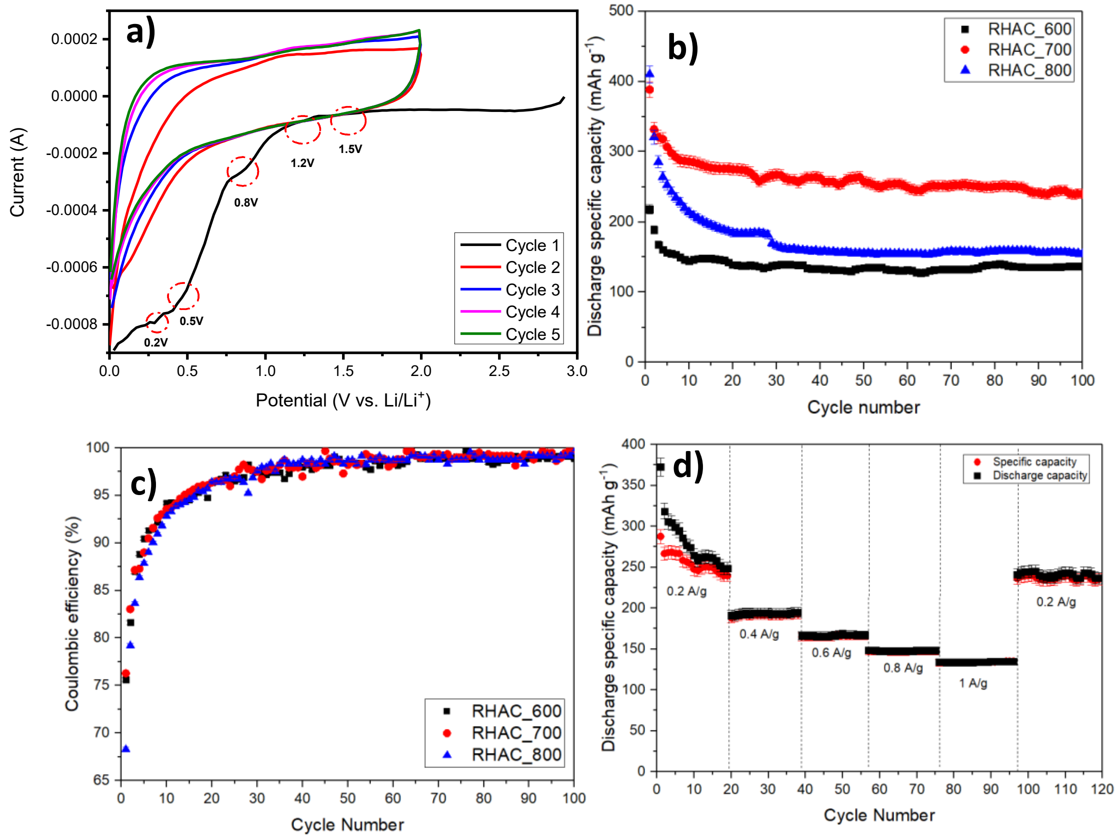

Figure 6. Electrochemical performance of RHAC as an anode material for LIBs. (a) CV curves of RHAC_700 for the first five cycles. (b) Cycling performance of RHAC_600, RHAC_700, and RHAC_800 half-cells measured at 0.01–2.0 V vs. Li/Li^+ and 0.2 A g^{-1}. (c) Coulombic efficiency of the RHAC electrodes. (d) Rate capability of RHAC_700 at various current densities. All data are presented as the mean of three independent cells (n = 3); error bars represent the standard deviation (SD), with SD < 5% for discharge capacity and ±0.2% for coulombic efficiency

Table 2. The electrochemical properties of carbonaceous materials from agricultural waste as anode materials for lithium-ion batteries

Anode materials	Electrolyte	Mass loading	Specific discharge capacity /current density / cycles / voltage window	Reference
Carbon from Loofah fiber	1.0 M $LiPF_6$ EC: DMC (1:1 by volume)	Average mass loading of 1-0-2.0 mg cm^{-2}	225 mAh g^{-1} at 0.15A g^{-1} for 200 cycles in a potential range between 0.01 V – 3.0 V	[47]
Activated carbon from banana peel	1.0 M $LiPF_6$ in EC:DEC (50:50; v/v)	1.0 mg cm^{-2}	272 mAh g^{-1} at 0.2 A g^{-1} for 200 cycles in a potential range between 0.01 V – 3.0 V	[48]
Activated carbon from rice husk	1.0 M $LiPF_6$ EC: DMC (1:1 by volume)	NA	253 mAh g^{-1} at 0.1 A g^{-1} for 400 cycles in a potential range between 0.0 V and 2.5 V	[33]
Honeycomb Activated carbon from Argan shell	1.0 M $LiPF_6$ EC: DMC (1:1 by volume)	NA	220 mAh g^{-1} at 50 A g^{-1} for 200 cycles in a potential range between 0.01 V – 3.0 V	[49]
Activated carbon from rice husk	1.0 M $LiPF_6$ EC: DMC (1:1 by volume)	0.95 ± 0.15 mg cm^{-2}	250.00 ± 7.33 mAh g^{-1} at 0.2 A g^{-1} for 100 cycles at 0.2 A g^{-1} in a potential range between 0.01 V–2.0 V	This work

Electrochemical impedance spectroscopy (EIS) serves as a powerful tool for examining the dynamic aspects of ion transport and charge transfer processes. The EIS parameters were extracted by fitting the Nyquist plots using a modified Randles equivalent circuit, consisting of solution resistance (R_s) in series with SEI resistance (R_{SEI}) and charge-transfer resistance (R_{ct}), each in parallel with a constant phase element (CPE), followed by a Warburg element (Z_w) to account for Li^+ diffusion. Fitting was performed using ZSimpWin software, and the fitting uncertainties for each parameter are reported in Table 3.

In Figure 7 (a and b), all curves exhibit a semicircle in the high-frequency region and a vertical line in the low-frequency region. The intercept on the Z' axis in the high-frequency region corresponds to the solution resistance (R_s) and cell contact resistance. The SEI resistance (R_{SEI}) and charge-transfer resistance (R_{ct}) at the electrode/electrolyte interface are presented by two semicircles. The inclined straight line observed at low frequencies represents the Li^+ diffusion-related Warburg impedance (Z_w). The constant phase element (CPE) refers to the double-layer capacitance at the SEI interface [50].

Based on Figure 7, the results show that R_{ct} values decrease with increasing activation temperature. The R_{ct} of RHAC_600 was significantly higher (1223.00 ± 20.00 Ω) than that of RHAC_700 (249.50 ± 22.00 Ω) and RHAC_800 (277.60 ± 20.00 Ω), which can be attributed to insufficient KOH activation at 600 °C. This low-temperature activation results in underdeveloped porosity, limited electrolyte accessibility, and poorly formed conductive pathways. Moreover, the carbon structure at this temperature retains excessive oxygen-containing functional groups and lacks interconnected hierarchical pores, leading to inefficient Li^+ diffusion and electron transport, as reflected by the higher solution resistance (R_s= 2.9 ± 0.20 Ω) and Warburg impedance (Z_w= 6519 ± 100.00 Ω) [23, 51].

After charge-discharge, the semicircles in the Nyquist plots decrease markedly, yielding R_{ct} values of 11.85 ± 0.60 Ω, 4.31 ± 0.20 Ω, and 18.15 ± 0.90 Ω for RHAC_600, RHAC_700, and RHAC_800, respectively, indicating an improved electrochemical response. Among the samples, RHAC_700 exhibits the lowest R_{ct} (4.31 ± 0.20 Ω), which is attributed to its spongy and uniform pore structure that provides efficient transport pathways for Li^+ ions and electrons. Activation at 700 °C achieves an optimal balance between pore development (390.33 m^2 g^{-1}) and partial graphitization, resulting in stable cycling performance. In contrast, the slightly higher R_{ct} observed for RHAC_800 (18.15 ± 0.90 Ω) reflects the reduced effectiveness of charge transfer caused by a partially collapsed pore structure and loss of active edge sites, leading to lower long-term capacity [12, 22]. As a result, RHAC_700 maintains a higher discharge capacity over repeated cycles, demonstrating that the optimized pore structure and balanced conductivity are critical for long-term electrochemical performance.

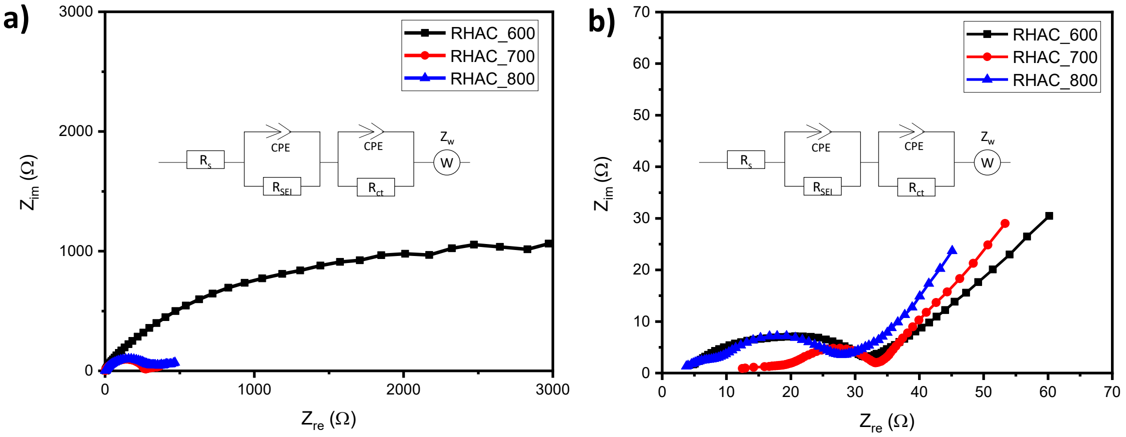

Figure 7. EIS spectra of RHAC electrodes measured (a) before and (b) after charge-discharge. Inset show (fitted equivalent circuit)

Table 3. The electrochemical parameters of RHAC electrodes measured from Nyquist plot before and after charge-discharge. Fitting errors (±) are reported to indicate the uncertainty of each parameter.

Before

Sample	**R_s (Ω)**	**R_{SEI} (Ω)**	**R_{ct} (Ω)**	**Z_w (S s$^{1/2}$)**	**χ^2**
RHAC_600	2.90 ± 0.20	370.20 ± 10.00	1223.00 ± 20.00	6519.0 ± 100.00	0.0026 ± 0.0005
RHAC_700	1.80 ± 0.10	16.66 ± 1.00	249.50 ± 22.00	0.0145 ± 0.001	0.0007 ± 0.0001
RHAC_800	1.28 ± 0.10	132.10 ± 5.50	277.60 ± 20.00	0.0175 ± 0.001	0.0013 ± 0.0002

After

Sample	**R_s (Ω)**	**R_{SEI} (Ω)**	**R_{ct} (Ω)**	**Z_w (S s$^{1/2}$)**	**χ^2**
RHAC_600	3.79 ± 0.20	15.50 ± 1.00	11.83 ± 0.60	0.0312 ± 0.002	0.0001 ± 0.00002
RHAC_700	14.61 ± 0.10	13.31 ± 0.80	4.31 ± 0.20	0.0511 ± 0.003	0.0025 ± 0.0005
RHAC_800	3.01 ± 0.20	5.64 ± 0.30	18.15 ± 0.90	0.0440 ± 0.003	0.0003 ± 0.00006

4. **Conclusion**

In this work, activated carbon derived from rice husk was successfully prepared via a microwave-assisted pyrolysis technique, followed by KOH activation at different activation temperatures of 600 °C, 700 °C and 800 °C. FESEM analysis reveals significant structural changes in the materials, with a greater number of active sites observed on the surface of RHAC_700 sample. This can be attributed to the complete pyrolysis of organic components in the rice husk, which creates efficient channels for lithium-ion and electron transport. The XRD and Raman results confirm that the graphitization of the carbon materials increased with the activation temperature. As a result, RHAC_700 electrodes demonstrate an initial discharge capacity of 388.33 ± 11.65 mAh g^{-1} with a Coulombic efficiency 68.29 % and stabilize at 250.00 ± 7.33 mAh g^{-1} with a Coulombic efficiency of 99.82% over 100 cycles at 0.2 A g^{-1} and 25 °C. Among the three electrodes, RHAC_700 electrode exhibits the lowest R_{ct} value of 4.31 ± 0.20 Ω, indicating a relatively higher electrical conductivity. The discharge capacity of 248.33 ± 7.45 mAh g^{-1} is maintained after 120 cycles when the current density is returned to the lowest current density of 0.2 A g^{-1}, signifying the RHAC_700 electrode had good electrochemical reversibility. Overall, RHAC_700 shows great promise as a sustainable anode material for lithium-ion batteries. Further studies focusing on detailed material characterization and full-cell testing are expected to provide deeper insights and enable continued performance optimization.

Declaration of AI and AI assisted technologies in the writing process

During the preparation of this work the author(s) used ChatGPT (GPT-4, OpenAI) in order to refine the academic language, improve sentence clarity, and assist with initial paraphrasing of certain methodology descriptions. After using this tool/service, the author(s) reviewed and edited the content as needed and take(s) full responsibility for the content of the publication

Declaration of Competing Interest

The authors declare that they have no known competing financial interests or personal relationships that could have appeared to influence the work reported in this paper.

Acknowledgements

The authors gratefully acknowledge Geran Penyelidikan Hi-Tech(F4) (Q.J130000.4654.00Q25) and UTM's internal research grant (Potential Academic Staff (PAS), Q.J130000.2754.04K23) for supporting this research.

References

[1] Dong, Y., Liu, C., Rui, M., Zhang, X., Guan, Y., Chen, L., Huang, Q., Wang, M., Su, Y., and Wu, F., Review on Graphite Anodes for Fast-Charging Lithium-Ion Batteries: Mechanism, Modification and Characterizations. *Advanced Functional Materials*, 2025, 2506190. https://doi.org/10.1002/adfm.202506190

[2] Zhao, H., Zuo, H., Wang, J., and Jiao, S., Practical application of graphite in lithium-ion batteries: Modification, composite, and sustainable recycling. *Journal of Energy Storage*, 2024, vol. 98, 113125. https://doi.org/10.1016/j.est.2024.113125

[3] Hossain, M.H., Chowdhury, M.A., Hossain, N., Islam, M.A., and Mobarak, M.H., Advances of lithium-ion batteries anode materials—A review. *Chemical Engineering Journal Advances*, 2023, vol. 16, 100569. https://doi.org/10.1016/j.ceja.2023.100569

[4] Nezafat, Z., Dong, Y., Nasrollahzadeh, M., Shafiei, N., Gharoubi, H., and Javanshir, S., Recent progresses in energy conversion and storage of agricultural waste-derived (carbon/nano) materials: a review. *Green Chemistry*, 2024. https://doi.org/10.1039/D3GC04332K

[5] Muraleedharan Pillai, M., Kalidas, N., Zhao, X., and Lehto, V.-P., Biomass-based silicon and carbon for lithium-ion battery anodes. *Frontiers in Chemistry*, 2022, vol. 10, 882081. https://doi.org/10.3389/fchem.2022.882081

[6] Shukla, S.S., Chava, R., Appari, S., and Kuncharam, B.V.R., Sustainable use of rice husk for the cleaner production of value-added products. *Journal of Environmental Chemical Engineering*, 2022, vol. 10, no. 1, p. 106899. https://doi.org/10.1016/j.jece.2021.106899

[7] Tharaka, D.N., Tissera, N.D., Priyadarshana, G., and Dahanayake, D., A Comprehensive Review of Hierarchical Porous Carbon Synthesis from Rice Husk. *Rice Science*, 2025. https://doi.org/10.1016/j.rsci.2025.04.009

[8] Kiono, B.F.T., Winoto, S.H., Suryo, M.S.K.T., and Lazuardi, D., Synthesis of Silica Gel From Rice Husk Ash for Sustainable Air Conditioning Requirements. *Advance Sustainable Science Engineering and Technology*, 2025, vol. 7, no. 4, p. 02504011-02504011. https://doi.org/10.26877/asset.v7i4.1944

[9] Longo, L., Baldassin, D., Di Michele, A., Bittencourt, C., Menegazzo, F., and Signoretto, M., Activation strategies for rice husk biochar: enhancing porosity and performance as a support for Pd catalysts in hydrogenation reactions. *Catalysis Science & Technology*, 2025, vol. 15, no. 17, p. 5101-5115. https://doi.org/10.1039/d5cy00242g

[10] Angellinnov, F., Subhan, A., Rengga, W.D.P., Jumari, A., and Syahrial, A.Z., Effect of Rice Husk Derived Activated Carbon Surface Coating on NMC 811 Characteristics and Performance as Lithium-ion Battery Cathode. *Results in Surfaces and Interfaces*, 2025, 100567. https://doi.org/10.1016/j.rsurfi.2025.100567

[11] Nilmoung, S., Limphirat, W., Siriroj, S., and Ausavasukhi, A., Rice husk-activated carbon (RHAC) composited with V_2O_5 for lithium-ion batteries. *Applied Physics A*, 2024, vol. 130, no. 5, p. 305. https://doi.org/10.1007/s00339-024-07470-2

[12] Hou, J., Mao, X., Wang, J., Liang, C., and Liang, J., Preparation of rice husk-derived porous hard carbon: A self-template method for biomass anode material used for high-performance lithium-ion battery. *Chemical Physics*, 2021, vol. 551, 111352. https://doi.org/10.1016/j.chemphys.2021.111352

[13] Kumar, R., Sahoo, S., Joanni, E., and Singh, R.K., A review on the current research on microwave processing techniques applied to graphene-based supercapacitor electrodes: An emerging approach beyond conventional heating. *Journal of Energy Chemistry*, 2022, vol. 74, 252-282. https://doi.org/10.1016/j.jechem.2022.06.051

[14] Brazil, T.R., Gonçalves, M., dos Anjos, E.G.R., de Oliveira Junior, M.S., and Rezende, M.C., Microwave-assisted production of activated carbon in an adapted domestic oven from lignocellulosic waste. *Biomass Conversion and Biorefinery*, 2024, vol. 14, no. 1, p. 255-268. https://doi.org/10.1007/s13399-021-02192-4

[15] Li, Z., Peng, K., Ji, N., Zhang, W., Tian, W., and Gao, Z., Advanced mechanisms and applications of microwave-assisted synthesis of carbon-based materials: a brief review. *Nanoscale Advances*, 2025. https://doi.org/10.1039/D4NA00701H

[16] Wong, P.S., Chong, W.W.F., Tan, J.P., Ariffin, N.A.A.M., Foo, C.Y., Idris, R., Woon, K.S., Wong, K.Y., Tee, W.H., and Mong, G.R., Microwave-Assisted Pyrolysis: A Review of Tailored Carbon Materials and Scale-Up Challenges. *Journal of Analytical and Applied Pyrolysis*, 2025, 107241. https://doi.org/10.1016/j.jaap.2025.107241

[17] Ke, L., Zhou, N., Wu, Q., Zeng, Y., Tian, X., Zhang, J., Fan, L., Ruan, R., and Wang, Y., Microwave catalytic pyrolysis of biomass: a review focusing on absorbents and catalysts. *npj Materials Sustainability*, 2024, vol. 2, no. 1, p. 24. https://doi.org/10.1038/s44296-024-00027-7

[18] Abderrahim, N., Mergbi, M., Amor, H.B., and Djellabi, R., Optimization of microwave assisted synthesis of activated carbon from biomass waste for sustainable industrial crude wet-phosphoric acid purification. *Journal of Cleaner Production*, 2023, vol. 394, 136326. https://doi.org/10.1016/j.jclepro.2023.136326

[19] Dan, E., McCue, A.J., Dionisi, D., and Fernández Martín, C., On the potential of microwave heating to convert waste into added-value chemicals and materials: a review. *Philosophical Transactions A*, 2025, vol. 383, no. 2297, p. 20240071. https://doi.org/10.1098/rsta.2024.0071

[20] Al-Janabi, S., Shabbani, H., Courtney, J.M., Barron, A.R., and Othman, M., Microwave-assisted enhanced activation of date palm leaf char for optimized CO_2 adsorption. *Scientific Reports*, 2025, vol. 15, no. 1, p. 34928. https://doi.org/10.1038/s41598-025-18683-7

[21] Wazir, A.H., Wazir, I.U., and Wazir, A.M., Preparation and characterization of rice husk based physical activated carbon. *Energy Sources, Part A: Recovery, Utilization, and Environmental Effects*, 2020, 1-11. https://doi.org/10.1080/15567036.2020.1715512

[22] Qin, Z., Ye, Y., Zhang, D., He, J., Zhou, J., and Cai, J., One/Two-Step Contribution to Prepare Hierarchical Porous Carbon Derived from Rice Husk for Supercapacitor Electrode Materials. *ACS omega*, 2023, vol. 8, no. 5, p. 5088-5096. https://doi.org/10.1021/acsomega.2c07932

[23] Nandi, R., Jha, M.K., Guchhait, S.K., Sutradhar, D., and Yadav, S., Impact of KOH activation on rice husk derived porous activated carbon for carbon capture at flue gas alike temperatures with high CO_2/N_2 selectivity. *ACS omega*, 2023, vol. 8, no. 5, p. 4802-4812. https://doi.org/10.1021/acsomega.2c06955

[24] Sugie, S. and Maeda, H., Conversion of rice husks into carbonaceous materials with porous structures via hydrothermal process. *Environmental Science and Pollution Research*, 2024, vol. 31, no. 33, p. 45711-45717. https://doi.org/10.1007/s11356-024-34217-6

[25] Liu, P., Sun, S., Huang, S., Wu, Y., Li, X., Wei, X., and Wu, S., KOH activation mechanism in the preparation of Brewer's spent grain-based activated carbons. *Catalysts*, 2024, vol. 14, no. 11, p. 814. https://doi.org/10.3390/catal14110814

[26] Yerdauletov, M.S., Nazarov, K., Mukhametuly, B., Yeleuov, M.A., Daulbayev, C., Abdulkarimova, R., Yskakov, A., Napolskiy, F., and Krivchenko, V., Characterization of Activated Carbon from Rice Husk for Enhanced Energy Storage Devices. *Molecules*, 2023, vol. 28, no. 15, p. 5818. https://doi.org/10.3390/molecules28155818

[27] Tang, S., Baker, G.A., Ravula, S., Jones, J.E., and Zhao, H., PEG-functionalized ionic liquids for cellulose dissolution and saccharification. *Green Chemistry*, 2012, vol. 14, no. 10, p. 2922-2932. https://doi.org/10.1039/C2GC35631G

[28] Chen, Z., Wang, X., Xue, B., Li, W., Ding, Z., Yang, X., Qiu, J., and Wang, Z., Rice husk-based hierarchical porous carbon for high performance supercapacitors: The structure-performance relationship. *Carbon*, 2020, vol. 161, 432-444. https://doi.org/10.1016/j.carbon.2020.01.088

[29] Surib, N.A., Khairunnisa, M., Lenggoro, I.W., Liza, S., and Wong, Y.H., Conductive particulate films fabricated by electrospray deposition of candle soot suspensions with acid treatment. *Advanced Powder Technology*, 2023, vol. 34, no. 9, p. 104107. https://doi.org/10.1016/j.apt.2023.104107

[30] Yu, K., Li, J., Qi, H., and Liang, C., High-capacity activated carbon anode material for lithium-ion batteries prepared from rice husk by a facile method. *Diamond and Related Materials*, 2018, vol. 86, 139-145. https://doi.org/10.1016/j.diamond.2018.04.019

[31] Guo, D., Xin, R., Zhang, Z., Jiang, W., Hu, G., and Fan, M., N-doped hierarchically micro-and mesoporous carbons with superior performance in supercapacitors. *Electrochimica Acta*, 2018, vol. 291, 103-113. https://doi.org/10.1016/j.electacta.2018.08.109

[32] Hossain, N., Nizamuddin, S., Griffin, G., Selvakannan, P., Mubarak, N.M., and Mahlia, T.M.I., Synthesis and characterization of rice husk biochar via hydrothermal carbonization for wastewater treatment and biofuel production. *Scientific reports*, 2020, vol. 10, no. 1, p. 18851. https://doi.org/10.1038/s41598-020-75936-3

[33] Ahmed, F., Almutairi, G., Hasan, P.M., Rehman, S., Kumar, S., Shaalan, N.M., Aljaafari, A., Alshoaibi, A., AlOtaibi, B., and Khan, K., Fabrication of a biomass-derived activated carbon-based anode for high-performance li-ion batteries. *Micromachines*, 2023, vol. 14, no. 1, p. 192. https://doi.org/10.3390/mi14010192

[34] Wang, J., Yang, Z., Pan, F., Zhong, X., Liu, X., Gu, L., and Yu, Y., Phosphorus-doped porous carbon derived from rice husk as anode for lithium ion batteries. *Rsc Advances*, 2015, vol. 5, no. 68, p. 55136-55142. https://doi.org/10.1039/C5RA08148C

[35] Kaur, P., Kaur, P., and Kaur, K., Adsorptive removal of imazethapyr and imazamox from aqueous solution using modified rice husk. *Journal of Cleaner Production*, 2020, vol. 244, 118699. https://doi.org/10.1016/j.jclepro.2019.118699

[36] Zulkornain, M.F., Normanbhay, S., Saad, J.M., and Zamri, M.F.M.A., Optimization of rice husk hydrochar via microwave-assisted hydrothermal carbonization: fuel properties and combustion kinetics. *Bioresource Technology Reports*, 2022, vol. 17, 100888. https://doi.org/10.1016/j.biteb.2021.100888

[37] Mahari, W.A.W., Azwar, E., Foong, S.Y., Ahmed, A., Peng, W., Tabatabaei, M., Aghbashlo, M., Park, Y.-K., Sonne, C., and Lam, S.S., Valorization of municipal wastes using co-pyrolysis for green energy production, energy security, and environmental sustainability: A review. *Chemical Engineering Journal*, 2021, vol. 421, 129749. https://doi.org/10.1016/j.cej.2021.129749

[38] Liang, C., Wang, P., Li, Y., and Yu, K., Biomass based composite used as anode materials: Porous ZnO anchored on the rice husk-derived carbon substrate for Li-ion batteries. *Materials Science and Engineering: B*, 2022, vol. 278, 115656. https://doi.org/10.1016/j.mseb.2022.115656

[39] Hastuti, E., Subhan, A., and Puspitasari, D., Synthesis of activated carbon derived from chicken feather for Li-ion batteries through chemical and physical activation process. *Materials for Renewable and Sustainable Energy*, 2021, vol. 10, 1-9. https://doi.org/10.1007/s40243-021-00198-6

[40] Azlan, F.N.M., Abdah, M.A.A.M., Tan, Y.S., Mustafa, M.N., Walvekar, R., and Khalid, M., Microwave-etched V_2C MXene-activated carbon hybrid as a high-performance anode material for lithium-ion batteries. *Journal of Energy Storage*, 2023, vol. 72, 108620. https://doi.org/10.1016/j.est.2023.108620

[41] Ji, Y., Ge, Z., Zhu, H., Duan, J., Wang, Y., Gu, Y., and Chen, Z., Constructing a high ion conductivity artificial SEI on biomass derived hard carbon for sodium ion battery. *Journal of Energy Storage*, 2025, vol. 127, 117167. https://doi.org/10.1016/j.est.2025.117167

[42] Van, C.D., Thi, T.T.L., Le Van, K., and Lee, M.H., Structural control of activated carbons derived from rice husks for sustainable and enhanced lithium-ion battery anodes. *Electrochimica Acta*, 2025, vol. 526, 146169. https://doi.org/10.1016/j.electacta.2025.146169

[43] Feng, D., Li, Y., Qin, X., Zheng, L., Guo, B., Dai, W., Song, N., Liu, L., Xu, Y., and Tang, Z., Biomass derived porous carbon anode materials for lithium-ion batteries with high electrochemical performance. *International Journal of Electrochemical Science*, 2024, vol. 19, no. 3, p. 100488. https://doi.org/10.1016/j.ijoes.2024.100488

[44] Dos Reis, G.S., Subramaniyam, C.M., Grimm, A., Hamedi, M.M., Molaiyan, P., García-Alvarado, F., Lassi, U., Goclon, J., and Petnikota, S., Biomass-derived macroporous carbon–tin oxide composites as stable and high-capacity anodes for lithium-ion and sodium-ion batteries: experimental study and GFN1-xTB calculations. *Physical Chemistry Chemical Physics*, 2025, vol. 27, no. 26, p. 14000-14014. https://doi.org/10.1039/D5CP01053E

[45] Kong, L., Zhu, Y., Williams, P.J., Kabbani, M., Brushett, F.R., and Rupp, J.L., Insights into Li+ storage mechanisms, kinetics, and reversibility of defect-engineered and functionalized multi-walled carbon nanotubes for enhanced energy storage. *Journal of Materials Chemistry A*, 2024, vol. 12, no. 7, p. 4299-4311. https://doi.org/10.1039/D3TA07362A

[46] Qiu, H., Yue, H., Zhang, T., Li, T., Wang, C., Chen, G., Wei, Y., and Zhang, D., Enhanced electrochemical performance of Li_2FeSiO_4/C cathode materials by surface modification with $AlPO_4$ nanosheets. *Electrochimica Acta*, 2016, vol. 222, 1870-1877. https://doi.org/10.1016/j.electacta.2016.11.180

[47] Wu, Z., Wang, L., Huang, J., Zou, J., Chen, S., Cheng, H., Jiang, C., Gao, P., and Niu, X., Loofah-derived carbon as an anode material for potassium ion and lithium ion batteries. *Electrochimica Acta*, 2019, vol. 306, 446-453. https://doi.org/10.1016/j.electacta.2019.03.165

[48] Luna-Lama, F., Morales, J., and Caballero, A., Biomass porous carbons derived from banana peel waste as sustainable anodes for lithium-ion batteries. *Materials*, 2021, vol. 14, no. 20, p. 5995. https://doi.org/10.3390/ma14205995

[49] Metyouy, K., Karbak, M., Ghamouss, F., and Chafik, T., Tuning the morphology of argan shells-based activated carbon towards applications as an anode for lithium-ion battery. *Diamond and Related Materials*, 2024, 111152. https://doi.org/10.1016/j.diamond.2024.111152

[50] Cheng, Y., Zhao, J., Zhang, L., Wan, J., Yang, J., and Wang, H., The effect of thermal treatment temperature on the crystal structure and electrochemical performance of the coconut shell-based

hard carbon. *Solid State Ionics*, 2023, vol. 402, 116374. https://doi.org/10.1016/j.ssi.2023.116374

[51] Mukhametgazy, N., Temirkulova, K.M., Balgabayeva, B., Khamzin, B.G., Azat, S., Supiyeva, Z.A., and Abbas, Q., Effect of Activating Agent and Temperature Conditions on the Electrochemical Performance of Rice Husk-Based Activated Carbon in Supercapacitors. *Eurasian Journal Of Chemisty* 2025, vol. 30, no. 2 (118), p. 62-73. https://doi.org/10.31489/2959-0663/2-25-3